Atomization and Sprays, vol. 2, pp. 463–481, 1992

ATOMIZATION, CHARGE, AND DEPOSITION CHARACTERISTICS OF BIPOLARLY CHARGED AIRCRAFT SPRAYS

K. D. Kihm, B. H. Kim, and A. R. McFarland
Department of Mechanical Engineering, Texas A&M University, College Station, Texas 77843

Atomization, charge, and deposition characteristics of a bipolar-charged electrostatic aircraft spray system were studied. The system used serrated spinner cup atomizers with tap water as the atomized fluid. Despite the well-known advantages of electrostatic sprays, electrical discharge from excessive buildup of residual charge on the aircraft skin has been a major problem in utilizing electrostatic systems for aircraft spraying. The idea of bipolar electrostatic charging has been investigated, and the results show that the bipolar charging could effectively abate the residual charge buildup. In addition, the deposition efficiency of aircraft sprays could be fairly significantly enhanced. Atomization and charging behaviors of the atomizer were studied under a laboratory simulation using a laser diffraction droplet sizing technique and a Faraday cage collector, respectively. The deposition characteristics were investigated by carrying out a field experiment with an aircraft spray system and a water-sensitive dye paper sampling technique. Droplet patterns on exposed dye papers were digitized and processed to obtain the droplet diameters and other statistical data. Compared with corresponding electrically neutral sprays, the average SMD of bipolar-charged sprays was increased by over 10%, with a noticeable decrease in the number of small droplets and an increase in large drops. The effect should reduce the drift problem of aircraft sprays. The total deposition mass was also increased by more than 45% when the spray was charged with dual polarities.

INTRODUCTION

Aircraft spray systems are widely used for applying pesticides to agricultural fields and hard-to-reach terrain such as mountain areas. In aerial spray applications, the drift of sprayed aerosols must be reduced so that air pollution problems are minimized and plant deposition is maximized. One way to achieve this goal is to charge sprays electrostatically, which enhances deposition by Coulomb attraction between a charge on the spray and its image charge on the ground targets [1]. Carlton and Bouse [2] demonstrated experimentally, with a ground-based electrostatic spray system, that the deposition efficiency can exceed its uncharged counterpart by as much as 800%. They also showed that tap water must be charged to a Q/M ratio larger than 5×10^{-3} C/kg to obtain the desirable increase in deposition.

For the case of aircraft application of the electrostatic sprays, where an aircraft releases unipolarly charged sprays, a surface charge of the opposite polarity develops on the aircraft skin. Excessive buildup of the surface residual charge creates an electric field

Financial support for the present work was provided by the U.S. Department of Agriculture through the Agricultural Research Service (ARS), College Station, Texas. The authors wish to thank L. F. Bouse and J. Carlton of the USDA-ARS for their many valuable suggestions and help throughout the work.

NOMENCLATURE

d	liquid drop diameter, μm	SMD	Sauter mean diameter ($=\sum_i N_i d_i^3/\sum_i N_i d_i^2$), μm
D	spinning cup diameter, m	T	temperature, K
e	charge of a single electron ($=1.602\times10^{-19}$ C)	U	velocity, m/s
E_0	electric field, V/m	VMD	volume mean diameter ($=\sum_i N_i d_i^3/\sum_i N_i)^{1/3}$, μm
k	Boltzmann constant ($=1.38\times10^{-23}$ J/K)	x	coordinate parallel to the spinning axis
l_c	characteristic length scale, m or mm	z	charge number
M	liquid mass, kg	β_{ij}	coalescence coefficient, cm^3/s
n	droplet concentration, cm^{-3}	γ_{ij}	diameter ratio
N	number of drops	ε_0	permittivity of free space ($=8.854\times10^{-12}$ F/m)
N_{ij}	number of collisions per unit time and per unit volume	μ	dynamic viscosity, Pa s
q_c	critical liquid feed rate for different disintegration modes using a serrated spinner atomizer, kg/s	ρ	density, kg/m^3
		σ	surface tension, N/m
		ω	spinner rotational rate, rad/s
q_p	charge per particle, C	**Subscripts**	
Q	liquiod volume flow rate, m^3/s, or charge amount, C	a	air
		l	liquid
r	coordinate perpendicular to the spinning axis	r	relative property

that can generate localized electric discharges. Since the electric discharge results in undesirable fluctuations in both charge distribution and electric field around the aircraft, a buildup of aircraft surface charge may degrade the deposition efficiency of charged sprays [3]. Also, the capacitive discharge from the residual charge on the aircraft while landing may have a potential hazard of explosion.

An idea that uses alternately charged nozzles has been proposed and investigated as a way to minimize or eliminate the buildup of aircraft surface charge so that electrostatic aircraft sprays can ensure an improved deposition efficiency. In addition, this approach offers a possibility of reducing spray drift, since oppositely charged sprays will coalesce, and the smaller spray particles will coalesce far more quickly than the larger ones because of the higher electric mobility of smaller droplets [4].

The present work consists of two basic parts: (1) a laboratory study of atomization and charge characteristics of spray droplets from a serrated spinning cup atomizer; and (2) a field study of spray deposition and coalescence characteristics of bipolar charge aircraft spray system. Both studies used tap water that was atomized with a serrated spinning cup atomizer. Spray charging was attained with an induction charging ring installed near the periphery of the spinning cup. A He-Ne laser Fraunhofer diffraction particle sizer, Malvern 2600 D system, was used to measure the spray size for the laboratory study. The amount of spray charge was measured by collecting charged sprays with a Faraday cage. For the aircraft spray field study, sprays were sampled with water-sensitive dye papers, and the exposed papers were digitized and processed for data analysis. Repeated measurements were made to ensure statistically valid and consistent experiments.

EXPERIMENTAL APPARATUS AND TECHNIQUES

Serrated Spinning Cup Atomizer

The spinner atomizing system is more convenient and lighter compared with other atomizer systems such as a pressure atomizer or a twin-fluid atomizer, since the latter systems require heavier pumps or compressors. Other important attributes of spinner atomizers are that the atomization characteristics can readily be controlled by regulating the liquid flow rate and the spinner rotational rate, and the spray drop diameters will have a fairly uniform distribution with a relatively small standard deviation [5].

The general configuration of a DC motor-driven spinning cup atomizer is presented in Fig. 1. The design of the atomizer is based on the work of Bals [6]. A laboratory-type atomizer, which had been designed by Carlton and Bouse [2], was employed for the present study. The cup has a dimension of 55 mm in diameter with 360 uniformly shaped triangular teeth with a serration pitch of 480 μm. The incorporation of teeth on the periphery improves the drop size uniformity [7]. The spinning cup rotates and receives water from the two brass tube outlets. Atomizer parts, other than the liquid passage, which was grounded, were made of nonconducting materials wherever possible to achieve high-voltage insulation and to minimize the electric field distortions and/or the electric discharge. A cylindrical and nonrotating charging electrode was installed to charge the liquid droplets inductively. The aluminum-made charging electrode has a dimension of 63 mm in outer diameter and 1.6 mm in thickness. The clearance between the charging ring and the spinner cup edge is approximately 2 mm in the axial direction and 2.4 mm in the radial direction. When a positive potential is placed on the charging ring and the negative terminal from a power supply is connected to the liquid outlets, droplets near the serrated periphery are negatively charged because of the electron induction mechanism, and vice versa for reversed polarities.

The first conventional work on the spinning cup atomizer was done by Hinze and Milborn [8]. Their work showed that the spray could be formed via three different modes: (1) by direct drop formation at the edge of the disk, (2) by the formation and breakup of liquid ligaments stretched away from the edge of the disk, and (3) by the formation and

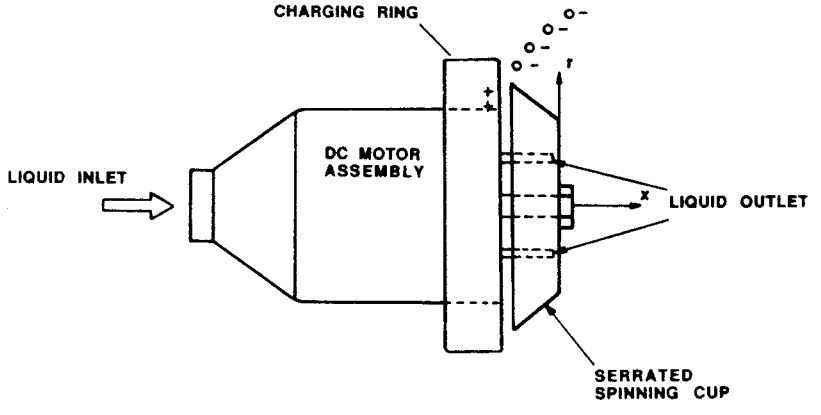

Fig. 1 Configuration of the motor-driven serrated spinning cup atomizer.

disintegration of a liquid sheet spreading radially from the edge. Transitions of the atomization modes can take place as the liquid flow rate is increased when other conditions are fixed [9]. For a given spinner rotational rate, when the feed rate is insufficient, the liquid cannot cover the entire surface of the spinner. The liquid leaves the teeth of the spinner in the form of dripping drops, which is called direct drop formation. Like the usual dripping of liquid, a significant number of secondary drops is formed in this mode. The standard deviation of the drop diameter distribution is generally large. As the feed rate increases, a thin liquid sheet covers the entire spinner surface and ligaments are formed at the spinner periphery that disintegrate into numerous drops. This mode is called a ligament disintegration, which is identical with the breakup of a straight liquid column and can be described by Rayleigh's instability theory [10]. The distribution of drop diameters becomes fairly uniform, with a minimal standard deviation and a minimal mean diameter. When the feed rate exceeds a critical value, the spinner surface is flooded and the liquid sheet extends outside the periphery. The extended sheet disintegrates into drops irregularly, which is called a sheet disintegration. The drop diameters become highly polydispersed because of the irregularity. Similar transition of the atomization modes will occur when the spinner rotational rate is decreased for a fixed liquid flow rate.

Figure 2 presents the critical feed rate for the transitions to the ligament disintegration mode (the dashed curve) and to the sheet disintegration mode (the solid curve). These predictions were based on their experimental extrapolations. Tanasawa et al. [7] proposed an empirical criterion to determine the transition from the direct drop formation to the ligament disintegration mode:

$$q_c = 2.8 \left(\frac{D}{\omega}\right)^{2/3} \left(\frac{\sigma}{\rho_l}\right) \left[1.0 + 10 \left(\frac{\mu_l}{\sqrt{\rho_l \sigma D}}\right)^{1/3}\right]^{-1} \tag{1}$$

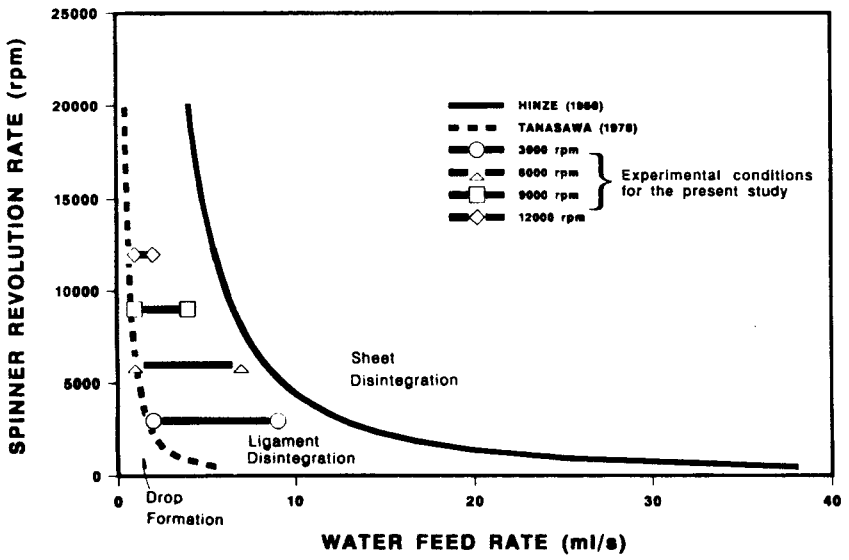

Fig. 2 Atomization modes of the spinner atomizer in terms of the rotational rate and the liquid feed rate.

where the critical feed rate, q_c, is a function of the spinning cup diameter, D, the rotational rate, ω, surface tension, σ, liquid density, ρ_l, and liquid viscosity, μ_l. Hinze [11] proposed a semiempirical criterion for the transition from the ligament disintegration mode to the sheet disintegration mode:

$$q_c = \left[1.77 \frac{\sigma D^3}{\rho_l} \left(\frac{\sigma}{\rho_l \omega^2 D^3}\right)^{0.6} \left(\frac{\rho_l \sigma D}{\mu_l^2}\right)^{0.167}\right]^{1/2} \tag{2}$$

The spinner disk operation was maintained in the ligamentary mode to assure the highest monodispersity and minimal spray diameters. The water feed rates for all the present experiments were adjusted within the ligament disintegration mode, as presented by the symbols and extended bars in Fig. 2.

Laboratory Setup

Figure 3 presents a schematic diagram of the laboratory experimental configuration. The spinning cup atomizer was fixed to spray boom section, which was located downstream of the air blower outlet. Tap water was fed through the boom. The blower outlet section had dimensions of 154 mm in diameter and 0.6 m in length., and contained a honeycomb-type flow straightener. Air was blown into the outlet through the reservoir with a squirrel cage-type blower driven by a 40-hp motor. The maximum air speed at the outlet was 175 km/h, which is approximately equal to the typical cruising speed of the spray aircraft [12].

The atomizer was installed 0.15 m downstream of the blower outlet, and both the atomizer and the outlet were vertically adjustable. The Malvern particle sizing unit was

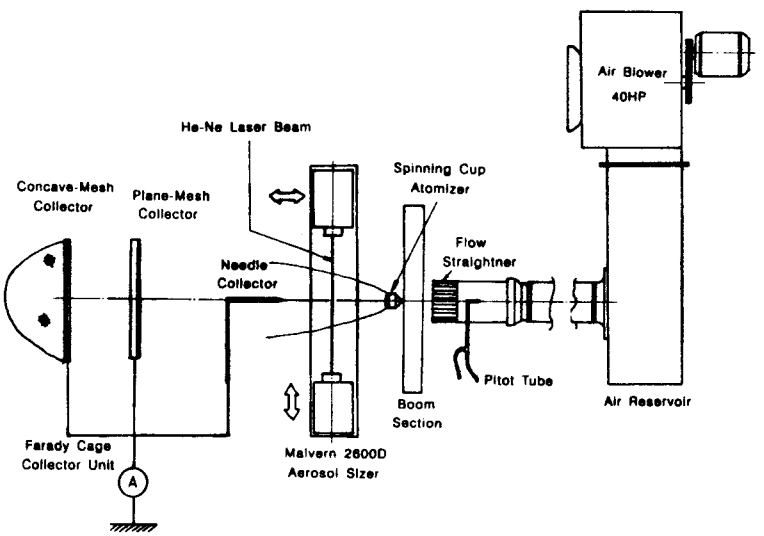

Fig. 3 Schematic diagram of experimental configuration for laboratory measurements of spray size and charge.

mounted on a horizontal two-dimensional positioning system. Thus, the whole system was capable of precise three-dimensional positioning of the atomizer. The Faraday cage unit consisted of three collector stages to maximize the collection efficiency: a needle collector, a plane-mesh collector, and a concave-mesh collector stage. The charge collection distribution for each collector stage was measured to be approximately 10%, 65%, and 25%, respectively. The meshes were 0.3-mm-diameter aluminum wires with a mesh size of 1.5 mm × 1.5 mm. All three stages were connected to a microamperemeter to measure the spray current.

Field Apparatus

A movable sampling stand, 60 m in length, was set up on a landing strip perpendicular to the aircraft cruising direction. The spray aircraft was flown in the upwind direction in an attempt to maximize the spraying period. Forty water-sensitive dye papers (25 mm × 75 mm each) were placed vertically at 0.5 m above the ground and at 0.6-m intervals along the stand. Ten atomizers were installed along a boom section attached behind the trailing edge of the right-hand wing of a Cessna model P-206B aircraft. The boom section was positioned close to the fuselage and away from the wing tip to minimize the influence of the wing tip vortex on the downstream aerial spray development [13, 14]. Wind speed and other atmospheric conditions, such as humidity and temperature, were measured and recorded with a portable weather station. The aircraft cruising altitude and indicated air speed during spraying were maintained at 3 m and 175 km/h, respectively.

RESULTS AND DISCUSSION

Results are presented for three different aspects of the study: (1) laboratory measurements of spray mean diameters for various atomizer operating conditions, (2) laboratory measurements of the amount of spray charge for different charging voltages, and (3) field measurements of spray deposition and size distributions.

Spray Mean Diameters

As illustrated in Fig. 4, a radially spiral spray is developed in the absence of an air stream while a hollow cone-type spray is formed under the action of a convective air stream. To account for such dramatically different spray developments, two different sampling locations were considered for the measurement of mean diameters. Point *A* was used when there was no superimposed air stream. The thickness of the radially developing spray was comparable to the probe beam diameter (9 mm) of the Malvern system. The droplet concentration was generally very low, and the beam center was matched with the midplane of the spray to obtain the maximum data rate. Location *A* was 150 mm radially away from the spinner axis. Under the action of the air flow, the spray was convected to form a hollow cone, and the spray thickness was again comparable to the laser probe diameter. The radial location of 27 mm was chosen to be equal to the spinner radius where the droplet concentration was a maximum. The axial location of 122 mm was determined as a location where the spray SMDs exhibited minimum values. (In selecting both locations *A* and *B*, the best effort was made to follow the recommendations established by ASTM E-29.04 subcommittee as published for Designation E1260-88 in Annual Book of

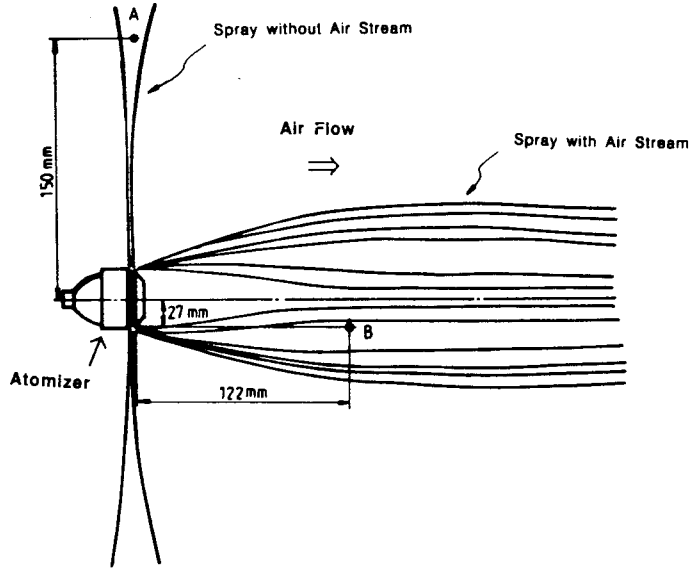

Fig. 4 Spray configurations and sampling locations for sprays without air flow (location *A*) and for sprays under convective air stream (location *B*).

ASTM Standards.) At both locations *A* and *B*, stable and highly repeatable values of Sauter mean diameter (SMD) were measured.

For the sprays without an air stream, variations of SMDs along different radial sampling locations are presented in Fig. 5. Results show that the SMD decreased grad-

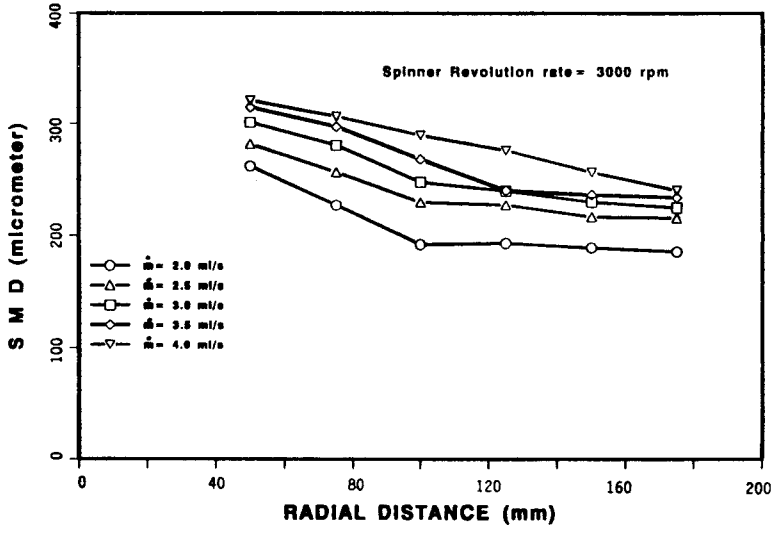

Fig. 5 Dependence of SMD on radial measurement locations with no convective air flow.

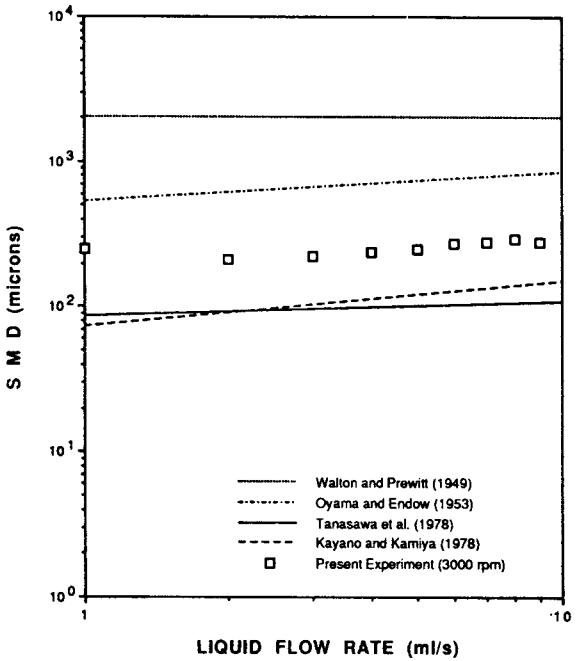

Fig. 6 Comparison of measured SMDs with theoretical predictions for 3000 spinner rpm.

ually and generally tended to reach a stable value as the sampling location was moved radially outward. For a centrifugal atomizer such as the spinner nozzle, drops with larger diameters carry higher centrifugal momenta and penetrate radially farther outward where the air speed is higher than inside the spray cone (Fig. 4). Weber number is estimated to be as large as 25 for the case of an air speed of $U = 50$ m/s and a maximum drop diameter of 500 μm that is comparable to the tooth size of the spinner. The estimated Weber number is above the critical Weber number, which is generally known to be of the order of 10. Thus secondary breakup may occur near the spray boundary for such extremely large drops. The evaporation rate on the droplet surface is also much higher near the spray boundary because of the high convective air flow and the lower vapor concentration than inside the spray. The gradual decrease in SMD along the radial direction may be attributed to the secondary breakup as well as to the evaporation on the droplet surface. As the water feed rate was increased, the radial location for which the SMD became stable moved farther from the spinner axis. Because longer and thicker ligaments are formed at the edge of the serrated teeth with an increase in feed rate, the spray development to a stable SMD was delayed to farther downstream.

A set of SMD data measured for the condition of $3k$ spinner rpm and without the air flow is presented as a function of the liquid feed rate in Fig. 6. The data are compared with SMDs calculated from several different extrapolated relations that describe the ligament atomization mode of spinning disk atomizers. Walton and Prewitt [15], who used a smooth disk and did not incorporate the effect of the liquid feed rate, presented an equation for maximum drop size:

$$D_{\max} = \frac{5.466}{\omega}\left(\frac{\sigma}{D\rho_l}\right)^{0.5} \tag{3}$$

Oyama and Endou [16] also used a toothless spinning disk atomizer and extrapolated an expression for the drop sizes:

$$\text{SMD} = \frac{1.112Q^{0.2}}{\omega D^{0.3}} \tag{4}$$

This equation contains no terms to denote liquid properties. Tanasawa et al. [7] proposed an equation that takes full account of atomization parameters including liquid properties:

$$\text{SMD} = 0.748\,\frac{Q^{0.1}\sigma^{0.5}}{\omega D^{0.5}\,\rho_l^{0.4}\,\mu_l^{0.1}} \tag{5}$$

Kayano and Kamiya [17] proposed another equation for mean drop size:

$$\text{SMD} = 0.0609\,\omega^{-0.79}\,Q^{0.32}\,D^{-0.69}\,\rho_l^{-0.29}\,(1 + 1.027\mu_l^{0.65}) \tag{6}$$

The discrepancies found between different data sets are due primarily to different spinner cup or disk configuration. Flat disk or cone configurations were used in their work, whereas the present atomizer used a rotating cup configuration with serrations. For the spinner rpms of $3k$, $6k$, $9k$, and $12k$ that were considered in the present investigation, the measured SMDs showed lower values than those predicted by Walton and Prewitt [15] and by Oyama and Endow [16], and larger values than Tanasawa et al. [7] and Kayano and Kamiya [17].

Measured data of SMD both with and without the air flow are presented in Fig. 7 as functions of liquid feed rate for four different spinner rotational rates. The symbols with dashed lines represent SMD values measured with a convective air stream of 175 km/h (or, equivalently, 49 m/s), and the symbols with solid curves represent data taken with no air flow. As the spinner rotational rate increases while the liquid feed rate remains unchanged (within the ligament breakup condition), the cross-sectional area of ligaments formed at the tips of serrated teeth of the spinner must be decreased because of mass continuity considerations. In primary atomization, ligament usually disintegrates into drops with sizes comparable to its own diameter. Therefore, reduced cross-sectional area of ligaments can explain the reduction in SMD when the spinner rotation is increased. The reduction in SMD with increased rpm occurred for both cases of with and without the convective air flow.

Because of the mass continuity, the ligament tends to be thickened whenever the liquid feed rate is increased for a fixed spinner rotational rate. For the case of no air flow, the gradual increase of SMD with the increase of liquid feed rate was attributed mainly to the enlargement of ligaments. When the cross-sectionally enlarged ligaments are exposed to a high-velocity air stream, however, viscous pulling action of the air may elongate the ligaments longitudinally, which can produce longer ligaments or nearly unchanged or even slightly reduced cross-sectional area. The independence of SMD on the feed rate with convective air stream may be explained by this unique atomization characteristic.

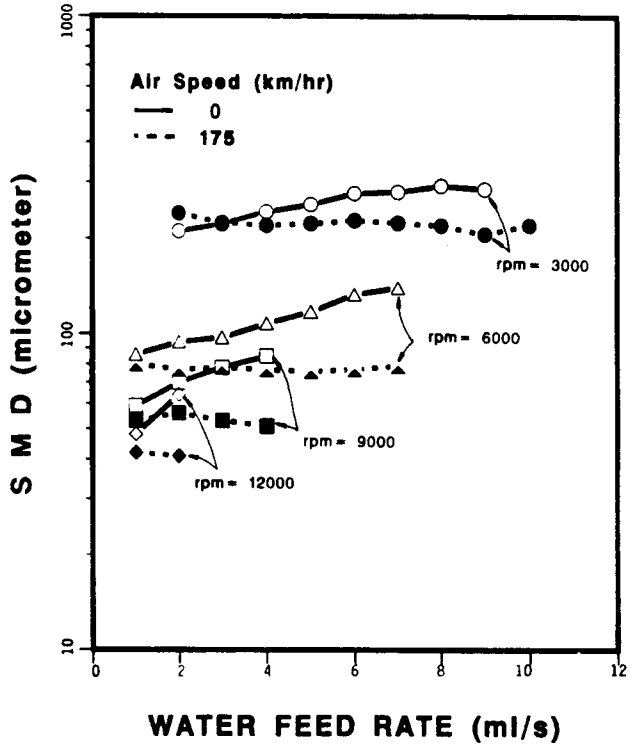

Fig. 7 Spray SMD both with and without the air flow versus water feed rate for four different spinner rotational rates.

Evaporation from the liquid surface by a high-speed air stream may also contribute to a further reduction in SMD. Sample calculations were made to estimate the droplet evaporation rate using the analysis reviewed by Lefebvre [5]. For example, for the case of water droplets of 100 μm at the ambient temperature and at 1 atm pressure exposed to a convective air stream of 50 m/s, the droplet lifetime can be as small as one-sixth of its counterpart under quiescent ambient air condition. This means that under convective air flow the volumetric evaporation rate is six times higher and the droplet diameter decreases almost twice faster ($6^{1/3}$) than in the case of no convection.

No significant secondary atomization of the primary droplets was expected unless the extremely large drops (some 3*k* rpm data) were exposed to the spray boundary, as discussed previously. The most ranges of measured droplet diameters were found to be already smaller than the critical diameters, where the critical diameter is that at which droplets break up due to the inertial stresses of the air stream overcoming the surface tension force. For liquids of surface tension is in the range of 0.028 to 0.475 N/m (0.073 N/m for pure water), Lane [18] has established an expression of:

$$d_{\text{crit}} = \frac{784}{U_r} \tag{7}$$

for the critical diameter, d_{crit}, in micrometers and the relative air speed, U_r, in meters per second. When a liquid with relatively low viscosity such as water is exposed to a strong convective air stream, Hinze [11] experimentally found a critical Weber number to have a value of 13, that is,

$$d_{crit} = \frac{13\sigma}{\rho_a U_r^2} \tag{8}$$

Richardson [19] derived a critical diameter by dimensional analysis of turbulence length scales considering a balance between the pressure force and the surface tension force:

$$d_{crit} = \left(\frac{\sigma l_c^{2/3}}{\rho_a U_r^2}\right) \tag{9}$$

where l_c is a characteristic length taken to be 150 mm that is equivalent to the air outlet diameter. The above three equations for the critical diameter estimation do not incorporate the viscosity contribution. The viscosity effects are important only for the microscale, much smaller than the typical length scale of liquid drops. The range of droplet diameters shown in Fig. 7 for an air speed of 175 km/h (49 m/s) are below or at best approximately equal to any of these estimated critical diameters. The probability of the secondary breakup, therefore, will be low for typical operation of the present spinner atomizer.

Spray charge

The charged spray is attracted to the induction charging ring of opposite polarity. As a result of this, charged sprays developed with larger spray cone angles compared with that of the uncharged spray. When there exist no or insufficient convective air flows, some charged droplets will deposit back on the induction charging ring and the deposited droplets will be conductively charged at the same polarity as the charging ring. These droplets then will be repelled from the charging ring and will carry charges of opposite polarity to that of the main spray. This phenomenon has been called a "reverse ionization" by Law and Bowen [20], and it acts to reduce the net charge of the spray. The convective air stream, or the aircraft cruising speed, must be above a certain level to prevent the reverse ionization.

Spray current (C/s or A) measured with the three staged Faraday cage collector is presented in terms of the charge-to-mass ratio, Q/M (C/kg) for various charging voltage levels in Fig. 8. Measurements were made for three different liquid feed rates (0.75 ml/s, 1.0 ml/s, and 1.5 ml/s). No significant difference was observed for different polarities of charging voltage. The typical charge-to-mass ratio increased by 25% when the spinner rotational rate was increased by 33% from 9*k* ro 12*k* rpm. The increased spinner revolution for a given liquid flow rate reduced the droplet SMD and increased the total surface area of spray droplets. The charge-to-mass ratio increased with the charging voltage and showed maximum values at approximately 7 to 8 kV. It decreases at higher voltages because of electrical breakdown [4], which results from an excessive electric field between the induction charging ring and the the water surface.

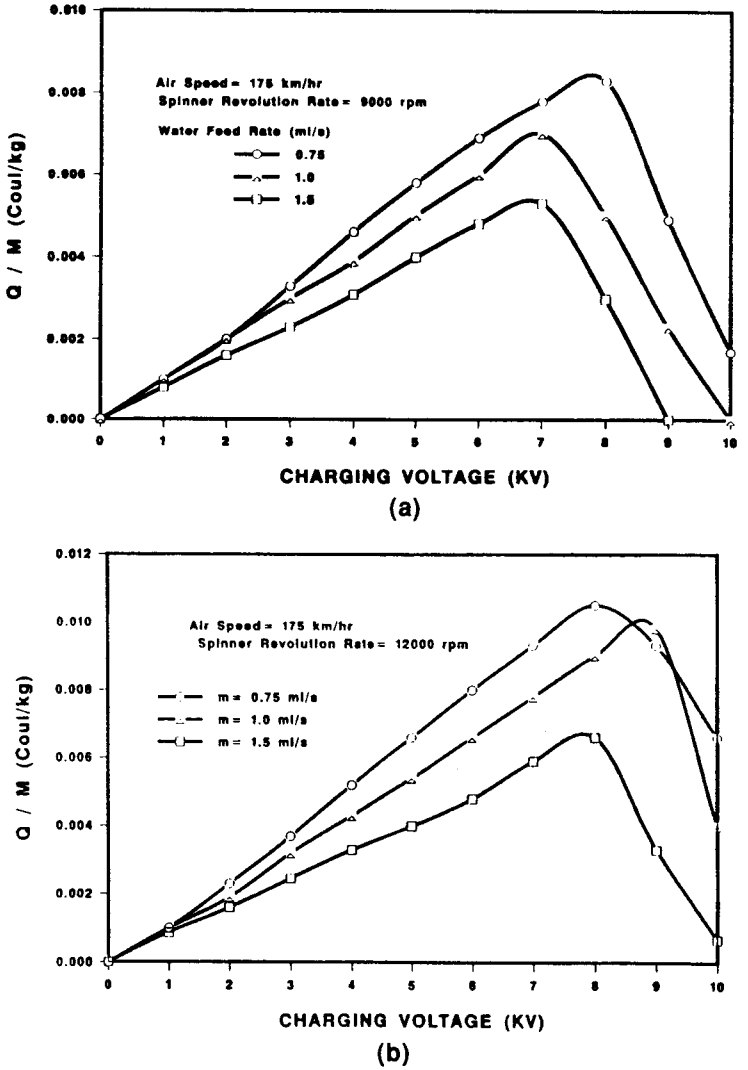

Fig. 8 Spray charge-to-mass ratio versus induction charging voltage for three different water feed rates for (a) 9000 spinner rpm and (b) 12,000 spinner rpm.

The charge-to-mass ratio decreases with increasing liquid flow rate. The saturated amount of induction charge on a spherical droplet of diameter d is expressed by [21]

$$q_p = \pi\varepsilon_0 (1.64 E_0 d^2) \tag{10}$$

where ε_o is the permittivity of free space (8.854×10^{-12} F/m) and E_0 denotes the impressed electric field. The induction charging is a surface phenomenon, and for unsaturated droplet the charge amount is assumed proportional to its surface area. Since the droplet diameter, d, remained nearly constant as the feed rate was increased (Fig. 7), the charge-to-mass ratio could be the same only if the individual droplet charge q_p is main-

tained at the same level for the case of increased flow rate. The level of the charge amount per drop, therefore, must have been reduced as the liquid flow rate was increased. This can explain the reduction in charge-to-mass ratio with increasing liquid feed rate. The atomization and charging mechanism of the present atomizer has shown to work best for a liquid flow rate of about 0.75 ml/s.

An excessively charged liquid drop can disintegrate into smaller droplets when the Coulomb repulsive force (the outward pressure produced by the surface charge) exceeds the restraining force (the inward pressure produced by the surface tension). This condition, the Rayleigh electrostatic limit [22], is expressed in terms of charge-to-mass ratio as

$$\frac{Q}{M} = \left(\frac{288\varepsilon_0\sigma}{\rho_l^2 d^3}\right)^{1/2} \tag{11}$$

When a charged spherical drop is in motion or exposed to a convective air stream, the geometric distortion into a prolate spheroid can result in decreasing the effective surface tension. This will reduce the charge required for the Rayleigh limit disintegration. Applying the analysis presented by Cerkanowicz [23] to typical experimental conditions of the present work (U = 50 m/s and d = 100 μm), the Rayleigh charge limit was shown to reduce to approximately one-half of the stationary Rayleigh limit. Although it is not shown, for the experimental results obtained herein the charge-to-mass values calculated based on the SMD were a factor of 10 below the electrostatic Rayleigh limit. The electrostatic charging, therefore, was not sufficient to lower the effective surface tension, and the spray SMD should not be altered significantly by the air flow, which was below the critical Weber number.

Results of SMD versus charging voltage are presented for two different spinner rotational rates and for three different liquid feed rates in Fig. 9. Up to the peak charging

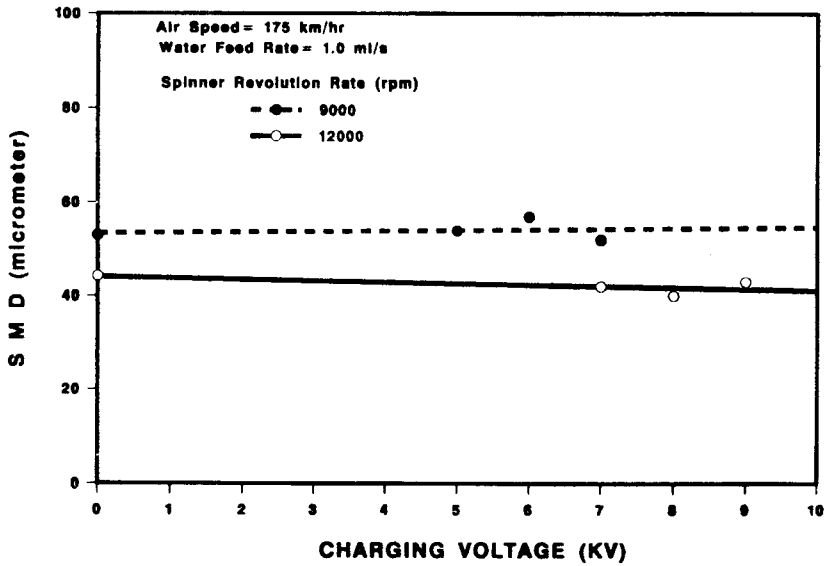

Fig. 9 Relationship of Spray SMD and charging voltage.

voltages corresponding to the maximum charge-to-mass ratio, the spray SMDs remained nearly unchanged for both spinner rotational rates. The results of Figs. 8 and 9 indicate that the droplet size and its formation are insensitive to the charging level, which is well below the Rayleigh limit.

Field Studies

For the field experiments, the liquid feed rate was maintained at 1 ml/s per atomizer, the rotational rates were set at 5*k* rpm and a charging voltage of 7 kV was used to provide a maximum value of the charge-to-mass ratio. An electric discharge pole was installed at each wing tip to monitor the electric current discharged to the environment. A reading of 25 μA of negative current was recorded when five sprays were unipolarly positively charged. When the other five sprays were activated with negative polarity, the reading was instantly decreased and a zero reading was attained. This proved that the bipolar electrostatic charged spray system eliminates any noticeable buildup of residual charge on the aircraft skin by neutralizing the residual charges of opposite polarities. Any temporary imbalance that may occur due to different operating conditions between the positive and the negative nozzles [24] has been carefully eliminated by slightly adjusting the power supply voltages.

The flight tests were repeated three times to ensure the consistency of the data. Each test consisted of three flights for neutral sprays and three flights for bipolar sprays. The bipolar spray droplets are larger and deposited more evenly than neutral sprays. These qualitative differences between the two sprays were quite consistent for all flight experiments. For quantitative analysis of the droplet deposition, the sizes of spots on the exposed water-sensitive dye papers were digitized through use of a video camera, intensified and processed using computer software to obtain necessary data including the number of drops, the number size distribution, the number median size, the SMD, and the volume mean diameter (VMD).

Figure 10 presents lateral distributions of the SMD and the number of deposited drops for both charged and uncharged cases. The average wind speed was 15 km/h, and the relative humidity was 26%. The zero lateral location was set at the centerline of the aircraft path. Since droplets will spread when they are collected by the water-sensitive dye paper, a spread factor must be considered in order to determine the true spray diameters. The spread factor is defined as the ratio of the marked diameter on the sampling paper to the spray droplet diameter. For the conditions of our experiment, a spread factor of 2 was used as suggested by the manufacturer [25]. The charged spray was more uniformly dispersed, showing less dependence of SMD and number count upon the lateral location. Also, the bipolar coalescence causes the mean diameter to increase, which can be explained by the preferential coalescence between the largest and smallest droplets.

The collision frequency of bipolar-charged droplets is expressed in terms of the concentrations of particles with diameter classes of d_i and d_j:

$$N_{ij} = \beta_{ij}\, n_i\, n_j \tag{12}$$

where N_{ij} represents the number of collisions occurring per unit time per unit volume between the two classes of particles of concentration n_i, and of concentration n_j of

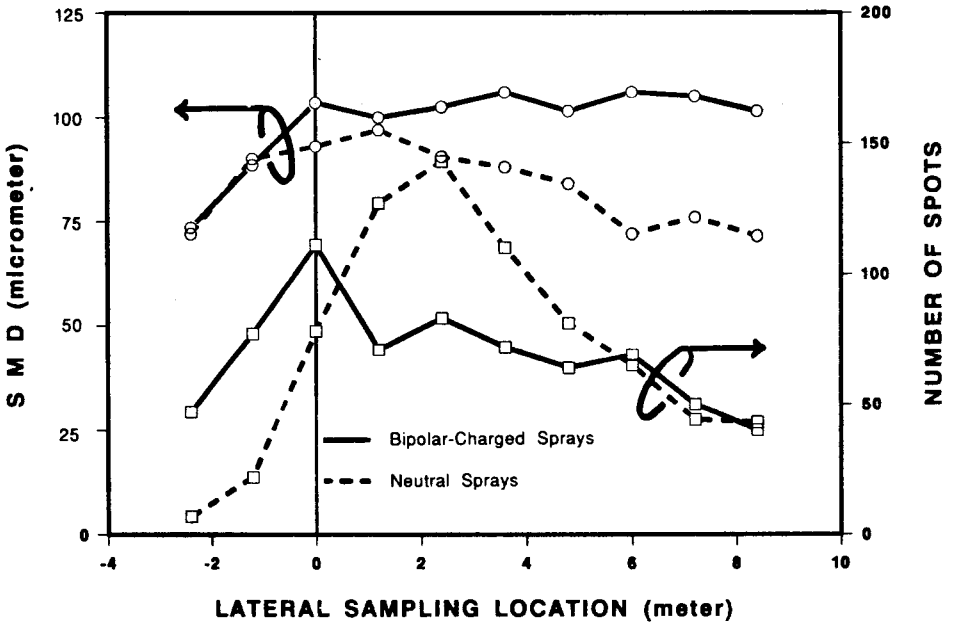

Fig. 10 Lateral distributions of SMD and the number of sampled drops for both dual-polarity charged and uncharged aircraft sprays.

opposite polarities. The coefficient β_{ij} is called a collision frequency function or coalescence coefficient and is expressed as [26]

$$\beta_{ij} = \left(\frac{4e^2}{3\mu_a\varepsilon_0}\right)\frac{z_i z_j}{d_j}\frac{(\gamma_{ij}^{-1}+1)}{\exp\left(\dfrac{2e^2}{\varepsilon_0 kT}\dfrac{z_i z_j}{d_j}\dfrac{1}{\gamma_{ij}+1}\right)-1}\times 10^6 \tag{13}$$

where μ_a denotes the air viscosity (1.85×10^{-5} Pa s at 300 K), ε_0 denotes the permittivity of free space (8.8542×10^{-12} F/m), k is the Boltzmann constant (1.38×10^{-23} J/K), and e is the elementary unit charge of an electron (1.692×10^{-19} C). The multiplication factor of 10^6 is used to provide units of cm^3/s for the coalescence coefficient, z_i and z_j represent the number of the unit charges (positive or negative) carried by droplets having diameters d_i and d_j, and γ_{ij} represents a diameter ratio defined as d_i/d_j. For uncharged particles, Eq. (13) reduces to an expression for the thermal coalescence coefficient due to Brownian motion of the two size classes [27], i.e.,

$$\beta_{ij} = \frac{2kT}{3\mu_a}\left(\frac{1}{d_i}+\frac{1}{d_j}\right)(d_i + d_j) \times 10^6 \tag{14}$$

The induction charging on a spherical particle is proportional to the surface area for the case of saturated charging:

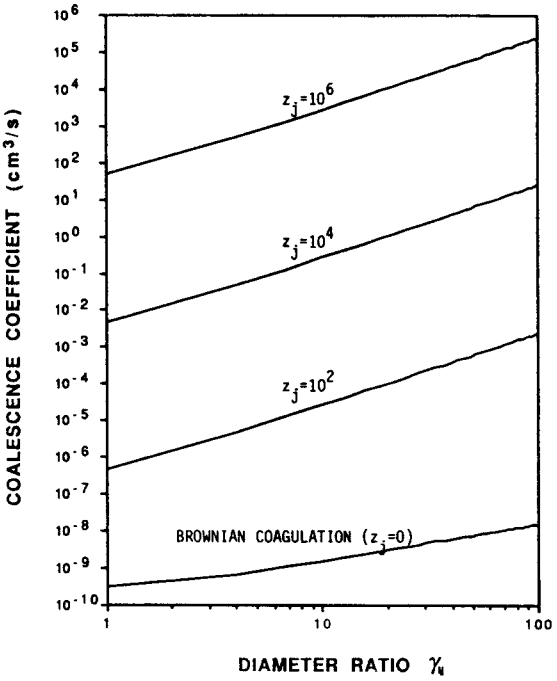

Fig. 11 Coalescence coefficient of bipolarly charged drops versus diameter ratio for a reference droplet of diameter, d_j, of 10 μm carrying a charge equivalent to $z_j e$ C.

$$z_i = \gamma_{ij}^2 z_j \tag{15}$$

The assumption of saturation charge is not always true, and the actual charging level will be lower as the drop diameter increases. It can be a reasonable deduction, however, to approximate that the induction charging below the saturation is also proportional to the surface area, since the induction charging is a surface phenomenon.

The coalescence coefficient of bipolar-charged sprays is expressed as

$$\beta_{ij} = -\left(\frac{4e^2}{3\mu_a \varepsilon_0}\right) \frac{z_j^2 \gamma_{ij}^2}{d_j} \frac{(\gamma_{ij}^{-1} + 1)}{\exp\left(\frac{2e^2}{\varepsilon_0 kT} \frac{z_j^2 \gamma_{ij}^2}{d_j} \frac{1}{\gamma_{ij} + 1}\right) - 1} \times 10^6 \tag{16}$$

Figure 11 presents calculated values of coalescence coefficient of Eq. (16) as a function of diameter ratio for several different charge numbers z_j. The reference diameter dj of 10 μm, which is nearly equal to the lower limit in the size spectrum, was considered in the calculation. The equivalent charge number, z_j, was calculated to be 1.63×10^5 for the medium range of charge-to-mass ratio, Q/M, of 0.005 C/kg (Fig. 8). The curve for zero charge number corresponds to the Brownian coalescence coefficient. The coalescence coefficient monotonically increases with increasing diameter ratio; i.e, the smaller droplets near the lower end of the size spectrum will preferentially coalescence with

bigger drops than with droplets of similar sizes. The coalescence preference for bigger drops increases as the diameter ratio increases. This preferential coalescence can explain the primary reason why the size spectrum of bipolarly charged sprays shifted to larger diameters compared with that of uncharged sprays.

The normalized size spectra of the deposited droplets for the three tests are presented in Fig. 12 for both charged and neutral sprays. The SMD values of the collected drops averaged for all three measurements were 92.4 μm for the neutral sprays and 105.1 μm for bipolarly charged sprays. It is apparent that for the case of the bipolarly charged sprays the size spectrum was shifted toward a larger mean value with a noticeable reduction in small droplets less than 50 μm in diameter and a significant increase in large drops (125 μm or more in diameter). Volume mean diameters were determined to be 82.7 μm and 94.2 μm for uncharged and charged sprays, respectively. By multiplying the VMD by the total particle count for each case, the ratio of deposited mass with bipolar charging to that without charging was determined to be 1.48. Thus, the deposited mass was increased by about 50% when bipolarly charged sprays were used. The gravitational settling velocity increases with the drop diameter squared, and the gravitational deposition rate will increase linearly with the settling velocity. The increased VMS of the bipolar sprays enhanced the settling velocity and the gravitational deposition by 30%, whereas the total 50% deposition enhancement was resulted by bipolarly charging sprays. The overall increase of deposition of the bipolar sprays, therefore, should be attributed to a combined result of the droplet coalescence and the electrostatic attractions.

The sampling paper technique has a resolution limitation for sampled droplets smaller than 30–40 μm, which are equivalent to the spray droplets ranging from 15 to 20 μm with a spread factor of 2. For neutral sprays, the result presented in Fig. 12 could have underestimated the number of small droplets and might have excluded droplets smaller than 15 μm. However, since the mass contributions of such small droplets are relatively

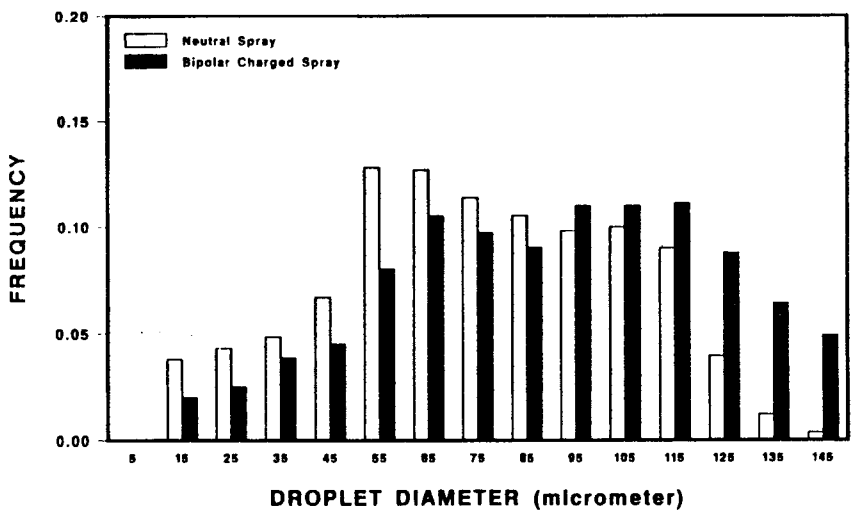

Fig. 12 Comparison of size distributions of neutral and bipolarly charged sprays. Data were obtained from field experiment.

small, results of both VMDs and the deposited mass should not have been much influenced by the limitation of the technique.

SUMMARY AND CONCLUSIONS

Characteristics of atomization, charging, and deposition were investigated for a bipolar electrostatic aircraft spray system. The system utilizes a serrated spinning cup atomizer. Both laboratory measurement and field experiment were carried out, and major conclusions of the study are as follows:

1. The SMD of atomized sprays was nearly constant for a range of liquid feed rates under convective air stream of 175 km/h, where the speed is typical of an agricultural spray aircraft.
2. The maximum value of the charge-to-mass ratio was measured to be of the order of 0.01 C/kg with a charging voltage of about 7 kV. The charge-to-mass ratio decreases with an increase of the liquid flow rate. The maximum charge-to-mass ratio was found to be an order of magnitude below the Rayleigh limit, and the spray SMD remained unchanged with an increase of the charging voltage.
3. A successful elimination of the buildup of residual charge on the aircraft skin was achieved with bipolar-charging of aircraft sprays.
4. Field studies showed the SMDs of deposited sprays were 15% larger for bipolarly charged sprays as compared with neutral sprays. A reduction in the number of small droplets and an increase in the number of large drops were noted when bipolar charging was used. This can be attributed to the coalescence of bipolarly charged sprays. The total amount of deposited mass was also increased by as much as 50% when the aircraft spray was bipolarly charged.

REFERENCES

1. C. N. Davies, *Aerosol Science*, Academic Press, New York, chap. 3, 1966.
2. J. B. Carlton and L. F. Bouse, Electrostatic Spinner-Nozzle for Charging Aerial Sprays, *Trans. ASAE*, vol. 23, no. 6, pp. 1369–1378, 1980.
3. J. B. Carlton and L. F. Bouse, Distribution of the Electric Field for an Electrostatic Spray Charging Aircraft, *Trans. ASME*, vol. 20, no. 2, pp. 248–357, 1977.
4. S. Oglesby and G. B. Nichols, *Electrostatic Precipitation*, Marcel Dekker, New York, chap. 2, 1978.
5. A. H. Lefebvre, *Atomization and Sprays, Hemisphere*, Washington, DC, pp. 127–134, 189–193, 222–228, and 309–366, 1989.
6. E. J. Bals, Design of Rotary Atomizers, *Proc, 4th Int. Agric. Aviat. Congr.*, Kingston, UK, pp. 156–165, 1969.
7. Y. Tanasawa, Y. Miyasaka, and M. Umehara, Effect of Shape of Rotating Disks and Cups on Liquid Atomization, *Proc. 1st Inst. Conf. Liquid Atomization and Spray Systems*, Tokyo, pp. 165–172, 1978.
8. J. O. Hinze and H. Milborn, Atomization of Liquids by Means of a Rotating Cup, *J. Appl. Mech.*, pp. 145–153, 1950.
9. L. S. Christensen and S. L. Steely, Monodisperse Atomizers for Agricultural Aviation Applications, NASA-CR-159777, 1980.
10. L. Rayleigh, On the Instability of Jets, *Proc. London Math. Soc.*, vol. 10, pp. 4–13, 1878.

11. J. O. Hinze, Fundamentals of the Hydrodynamic Mechanism of Splitting in Dispersion Processes, *AIChE J.*, vol. 1, no. 3, pp. 289–295, 1955.
12. H. O'Neal and R. W. Brazelton, Aerial Application of Pesticides, Report no. ADP 84-016, Shell Chemical Company, p. 22, 1984.
13. W. H. Reed, An Analytical Study of the Effect of Airplane Wake on the Lateral Dispersion of Aerial Sprays, NACA-Report 1196, 1954.
14. D. J. Morris, C. C. Croom, C. P. van Dam, and B. J. Holmes, An Experimental and Theoretical Investigation of Deposition Patterns from an Agricultural Airplane, NASA-TP-2348, 1984.
15. W. H. Walton and W. C. Prewitt, *Proc. Phys. Soc.*, London, Sec. B, vol. 62, p. 341, 1949.
16. Y. Oyama and K. Endou, On the Centrifugal Disk Atomization and Studies on the Atomization of Waterdrops, *Kogaku Kogaku*, Japan, vol. 17, pp. 256–260 and 269–275, 1953.
17. A. Kayano and T. Kamiya, Calculation of the Mean Size of the Droplets Purged from the Rotating Disk, *Proc. 1st Int. Conf. Liquid Atomization and Spray Systems*, Tokyo, pp. 133–138, 1978.
18. W. R. Lane, Shatter of Drops in the Stream of Air, *Ind. Eng. Chem.*, vol. 43, no. 6, pp. 1312–1317, 1951.
19. S. M. Richardson, *Fluid Mechanics*, Hemisphere, Washington, DC, pp. 260–264, 1989.
20. S. E. Law and H. D. Bowen, Charging Liquid Spray by Electrostatic Induction, *Trans. ASAE*, Paper no. 64-160, pp. 501–506, 1966.
21. J. A. Cross, *Electrostatics*, Adam Hilger, Bristol, England, pp. 198–218, 1987.
22. L. Rayleigh, On the Equilibrium of Liquid Conducting Masses Charged with Electricity, *Phil. Mag.*, vol. 14, pp. 184–186, 1882.
23. A. E. Cerkanowicz, Rayleigh Limit for Nonstationary Charged Drops, *IEEE Industry Applications Society Conference Proc.*, Paper no. 81C1678-2, pp. 1161–1165, 1981.
24. I. I. Inculet and J. K. Fischer, Electrostatic Aerial Spraying, *IEEE Trans. Ind. Appl*, vol. 25, no. 3, pp. 558–562, 1989.
25. Water-Sensitive Paper for Monitoring Spray Distribution, Operation Manual, Spraying Systems Co., Wheaton, IL, 1985.
26. G. M. Hidy, *Aerosols*, Academic Press, Orlando, FL, pp. 125–132, 1984.
27. S. K. Friedlander, *Smoke, Dust and Haze*, John Wiley, New York, chap. 7, 1977.